NJC

Optimization of the Synergistic Effects in Polycrystalline Pt-Au Electrodes in Developing an Effective Arsenic Sensor via Oxidation Reactions

Journal:	*New Journal of Chemistry*
Manuscript ID	NJ-ART-07-2024-003312.R1
Article Type:	Paper
Date Submitted by the Author:	12-Sep-2024
Complete List of Authors:	Hossain, Mohammad Imran; Shahjalal University of Science and Technology, chemistry Saha , Surove; Shahjalal University of Science and Technology, Chemistry Aoki, Kentaro; Japan Advanced Institute of Science and Technology, Materials Science Alam, Md. Mahfujul; Shahjalal University of Science and Technology, chemistry Singha, Nayan; Government College of Engineering and Leather Technology, Polymer Science and Technology Rahaman, Mostafizur; King Saud University, Chemistry Aldalbahi, Ali; King Saud University, Chemistry Nagao, Yuki; Japan Advanced Institute of Science and Technology, School of Materials Science Hasnat, Mohammad; Shahjalal University of Science and Technology; Shahjalal University of Science and Technology,

Optimization of the Synergistic Effects in Polycrystalline Pt-Au Electrodes in Developing an Effective Arsenic Sensor via Oxidation Reactions

Mohammad Imran Hossain [a], Surove Rani Saha [a], Kentaro Aoki [b], Md. Mahfujul Alam [a], Nayan Ranjan Singha [c], Mostafizur Rahaman [d], Ali Aldalbahi [d], Yuki Nagao [b], Mohammad A. Hasnat [a, e, *]

[a] *Electrochemistry & Catalysis Research Laboratory (ECRL), Department of Chemistry, School of Physical Sciences, Shahjalal University of Science and Technology, Sylhet-3114, Bangladesh*

[b] *School of Materials Science, Japan Advanced Institute of Science and Technology, 1-1 Asahidai, Nomi, Ishikawa 923-1292, Japan*

[c] *Advanced Polymer Laboratory, Department of Polymer Science and Technology, Government College of Engineering and Leather Technology (Post-Graduate), Kolkata-700106, West Bengal, India*

[d] *Department of Chemistry, College of Science, King Saud University, P.O. Box 2455, Riyadh 11451, Saudi Arabia*

[e] *International Research Organization for Advanced Science and Technology (IROAST), Kumamoto University, Kumamoto 860-8555, Japan*

***Corresponding Author:** Mohammad A. Hasnat (Email: mah-che@sust.edu)

Abstract

A detailed kinetic study of the electrocatalytic oxidation of arsenite [As(III)] to arsenate [As(V)] has been performed in acidic medium by using gold (Au) immobilized platinum (Pt) electrodes. To prepare the Au modified Pt electrodes, a polycrystalline Pt electrode was cycled between 0 to −1 V vs. Ag/AgCl (sat. KCl) in 0.05 M $HAuCl_4$ solution at a scan rate of 0.1 Vs^{-1}. The Pt-Au electrode prepared by 1 deposition cycle of Au demonstrated an As(III) oxidation peak potential at 0.79 V with a peak current value of 62.14 μA. As the deposition cycle was increased, the

required potential for oxidation reaction decreased shifting towards a more negative value. The least potential required was observed for the electrode prepared with 8 deposition cycles of Au. The result was also verified with various surface characterization techniques including SEM, EDX, XRD, and XPS. Kinetic investigation revealed that the As(III) ions approach the 8 cycles of Au deposited Pt electrode through a diffusion-limited process, subsequently following a first-order reaction with stepwise transfer of electrons. The electrode exhibited a sensitivity of 23.13 μA mM^{-1} for As(III) oxidation. The LOD for As(III) by the proposed electrode was found to be 65.39 μM which also boasts its excellent performance.

Keywords: Arsenite oxidation; Arsenic sensor; Pt-Au electrode; Electrodeposition; Kinetics; Catalysis

1. Introduction

Arsenic (As) is a naturally occurring element found in rocks, soil, water, and air, which is a metalloid with properties of both metals and non-metals.[1] It can form both organic and inorganic compounds, with inorganic arsenic being more prevalent.[2] It has been identified that even low concentrations of arsenic are extremely toxic, raising potentially severe environmental implications on a global scale.[3] The toxicity and mobility of arsenic change depends on its chemical form and valence state.[4] The World Health Organization (WHO) acknowledged that the maximum amount of arsenic that can be present in drinking water is 10 μg/L.[5] Due to high concentration of As in groundwater, more than 100 million people could be at risk in Bangladesh, India, China, Taiwan, Canada, southwestern states of the United States (like Nevada) including New England, Michigan, Minnesota, Wisconsin, and the Dakotas.[6,7] Arsenic exposure is primarily caused by oral contact with contaminated water, soil, agricultural, and seafood items, affecting people through mouth, nose, and skin.[8] Arsenic exposure can lead to hearing loss, diabetes, developmental abnormalities, neurological issues, cardiovascular illness, and disorders in various systems, mainly through oral intake.[9] Due to the severe toxicity and ubiquitous presence of arsenic, there is an urgent need for novel approaches to monitor and remove it from water bodies.

In laboratory settings, a wide array of instrumental methods is employed to detect arsenic. Among these, the most sensitive, selective, and accurate are atomic absorption spectrometry (AAS),[10] atomic fluorescence spectrometry (AFS),[11] laser-induced breakdown spectroscopy (LIBS),[12] and inductively coupled plasma-optical emission spectrometry/mass spectrometry (ICP-OES/MS).[13] For arsenic speciation analysis, highly efficient liquid chromatography and capillary electrophoresis are used in combination with these techniques.[14,15] Although these methods offer extensive analytical capabilities, they are predominantly suited for laboratory environments. Their high sensitivity to interference, complex sample preparation requirements, significant costs, and need for highly skilled operators limit their use in routine field monitoring of numerous samples. For this reason, research on electrochemical techniques has emerged as a crucial solution for quick, affordable, dependable, and portable method.[16] Electrochemical methods are ideal for in-situ monitoring of contaminated samples, creating portable circuits for online monitoring, and offer quick analytical reports compared to other spectroscopic techniques.[17,18] Electrochemical oxidation of As(III) using various materials are well documented in the literature. For example, Mahbubul *et al.* has demonstrated electrokinetics of arsenic oxidation reaction and the corresponding sensing activities by using Pd nanoparticles immobilized on a Pt surface in the presence of sodium dodecyl sulfate (SDS) molecules.[19] The experimental results showed that the charge transfer resistance and catalytic efficiency increased in the order of Pt < Pt–Pd < Pt–Pd_{sds} at the Fe(II)/Fe(III) couple's redox potential. Additionally, Mohebul *et al*. have shown how electropolymerized coating of poly(*o*-aminophenol) on the surface of Pt create a reliable sensor for the detection of As(III) in an acidic medium.[20] First-order kinetics governed the As(III) oxidation reaction at poly(*o*-aminophenophenol) modified Pt electrode, which had a mixed mechanistic pathway and two electron transfers to convert to As(V). Furthermore, various studies of As(III) oxidation have been done using Au electrodes also. Such as Ahsan *et al.* has performed a detailed kinetic investigation of As(III) oxidation which was performed on Au surface within the pH range between 3.0 and 9.0.[21] It was found that the As(III) oxidation on the As surface followed a purely adsorption-controlled process irrespective of pH values. Yan Liu *et al*. has introduced a electro-reduced graphene oxide (ERGO)-Au nanoparticles (AuNPs) composite film which was electrodeposited on a glassy carbon electrode (GCE) by cyclic voltammetry method.[22] The fabricated ERGO-AuNPs/GCE was employed to determine trace As(III) in 0.20 M aqueous HCl medium by anodic

stripping voltammetry (ASV). Idris *et al.* has presented the use of Au nanoparticles (AuNPs) modified glassy carbon electrodes for the electrochemical detection of arsenic, demonstrating increased redox current and improved detection using square wave anodic stripping voltammetry (ASV) under optimized conditions.[23]

Even though a significant number of articles have been published on oxidation of As(III), Pt and Au based electrodes either alone or combining with other materials, the synergistic effects generated by combining Pt and Au particles in oxidizing As(III) has to be explored yet. Pt-Au combination ought to exhibit better performance, since Pt and Au both individually demonstrate effective performance in the electrochemical oxidation of As(III). This is where the goal of the present research began. In this work, the electrochemical oxidation of As(III) in an acidic solution was investigated using an Au-deposited Pt electrode. Note that both Pt and Au particles are polycrystalline in nature having different crystal facets such as (111), (200) etc. However, roles of these crystal facets, particularly in the bimetallic form, on As(III) oxidation is still undiscovered. The population of these crystal facets in a Pt-Au electrode matrix could be controlled by controlling the contents of Au particles on a polycrystalline Pt surface. This is because the surface energy of Au on Pt electrode is influence by different Au content, leading to the preferential formation of one facets over other.[24] Suitable crystal facets with favorable adsorption energy can significantly enhance the electrocatalytic performance of an electrode.[25–27] In order to achieve the minimal requirement of potential with optimal current output for the electrochemical oxidation of As(III), the most effective fabrication of Au thin film on a polycrystalline Pt surface in which the population of (111) and (200) facets are optimized, was investigated. Thus, this study aims to enhance the performance of a polycrystalline Au modified Pt electrode by optimizing the deposition cycle of Au particles on Pt substrate to attain the best working electrode for electrooxidation of As(III) in an acidic solution.

2. Experimental

2.1. Materials and chemicals

0.1 M As (III) stock solution was prepared by dissolving an appropriate amount of sodium arsenite ($NaAsO_2$) (purchased from Merck KGaA 64271 Darmstadt, Germany) in Millipore Milli-Q water (resistivity less than 18 MΩ cm) (Smart-Q30UT deionized water system, Qingdao, Shandong, China). Tetrachloroauric acid ($HAuCl_4$), which was the precursor of Au particles, was

sourced from Aldrich Chemical Company to modify the Pt electrode. Sulfuric acid (H_2SO_4), NaOH, EtOH, acetone and alumina powder (Al_2O_3) were also procured from Aldrich Chemical Co. Inc., Germany. All the chemicals used in this study were of analytical grade reagent and used as received without further purification.

2.2. Electrode cleaning and modification

A polycrystalline Pt electrode with an exposed geometric area of 0.0314 cm^2 was first scrubbed clockwise and anti-clockwise in the aqueous slurries of fine alumina powder (average particle diameter 0.06 μm) and washed thoroughly with deionized water. Then the Pt electrode was sonicated for 10 minutes in 0.1 M H_2SO_4 to remove the adsorbed organic and inorganic impurities. The sonicated Pt surface was cleaned electrochemically in 0.1 M H_2SO_4 solution by repeatedly scanning for 20 cycles in the potential range from – 0.2 to +1.5 V at 0.1 Vs^{-1} scan rate until cyclic voltammetric characteristic peaks for a clean Pt electrode was obtained. The Au electrode was cleaned following the procedure mentioned in the literature [21].

The Au particles were deposited on the electrochemically cleaned Pt electrode by cycling the cleaned Pt electrode in $HAuCl_4$ solution. To perform electrodeposition, the Pt electrode was dipped into a 5 mL solution of 0.05 M $HAuCl_4$. Next, the Pt electrode was cycled between 0 and −1.0 V for 1 cycle at a scan rate of 0.1 Vs^{-1} using cyclic voltammetry method. This resulted the electro-deposition of Au particles on the Pt surface. Before applying for As(III) oxidation, the as-prepared Pt-Au electrode was washed thoroughly with distilled water and dried. To explore the optimized deposition layer of Au particles, the electro-deposition process was repeated for a series of cycles.

2.3. Electrochemical measurements

All electrochemical experiments were conducted with two potentiostats, CHI602E electrochemical workstation (CH Instruments, USA) and PGSTAT 128N (Autolab, Netherlands) employing a conventional three-electrode system. Au modified Pt electrode was used as the working electrode. An Ag/AgCl (saturated with KCl) and a Pt electrode were used as reference and counter electrodes, respectively. Linear polarization curves were obtained for open circuit potential (OCP) measurement for bare Pt, bare Au and Pt-Au electrodes in presence and absence of As(III) using 10 mL 0.1 M H_2SO_4 as the supporting electrolyte. The cyclic voltammograms

(CVs) were taken varying the cycles of Au deposition in a potential above the OCP value. The lower limit of potential scanning range was restricted to 0 V to avoid the electro-reduction of arsenic.

2.4. Instruments for characterization

The morphology of various electrode was analyzed using a scanning electron microscope (SEM) (JSM-7610F, Japan). X-ray diffraction (XRD) patterns were acquired with a Rigaku SmartLab diffractometer employing Cu Kα radiation (λ = 1.5406 Å). Le Bail fitting of XRD patterns were carried out using TOPAS3 (Bruker AXS) to get insight into the growth of the Au crystallite size and possible change in lattice parameters. Energy dispersive X-ray (EDX) analysis was performed using a TM3030Plus miniscope (Hitachi Ltd.). To determine the chemical states of Pt and Au on Pt-Au electrode, X-ray photoelectron spectra (XPS) were recorded with a delay-line detector (DLD) spectrometer (Kratos Axis Ultra; Kratos Analytical Ltd.) using an Al Kα radiation source (1486.6 eV). The XPS instrument was calibrated to 284.5 eV (C 1s).

3. Results and discussion

3.1. Catalyzing As(III) oxidation reaction

Variation in cyclic voltammetric peak potential (E_p) and peak current (I_p) for As (III) oxidation reaction were observed when number of Au deposition CV cycle was varied on Pt electrode, as shown in **Figure 1A**. The figure displays that with each consecutive Au deposition cycle, the E_p decreases gradually (negative shifting). The lowest E_p value of 0.639 V was achieved after coating the Pt electrode with 8 CV deposition cycles of Au. Intriguingly, beyond the 8th deposition, a shift was observed: E_p began to rise while I_p steadily declined. By the 9th cycle, E_p and I_p shifted slightly to 0.640 V and 59.51 μA, respectively. This trend became more pronounced after the 10th deposition, where E_p substantially increased to 0.714 V, and I_p decreased to 54.91 μA. The highest I_p was observed for 4 CV cycles of Au deposition on Pt electrode, also denoted as $(Pt\text{-}Au)_4$. **Figure 1C** presents a bar chart illustrating the variations in onset potential (E_i), peak potential (E_p), and peak current (I_p) over 1 to 10 cycles of Au deposition, where a decreasing trend in E_i and E_p and an increase in I_p are observed up to 8 cycles, followed by the onset of a reverse trend thereafter. **Figure 1B** demonstrates the performance of $(Pt\text{-}Au)_8$ in comparison to a bare Au and a bare Pt electrodes for As(III)

oxidation reaction. The $(Pt\text{-}Au)_8$ electrode outperforms the both electrodes in terms of higher peak current (I_p) and lower peak potential (E_p). **Table 1** summarizes the E_i, I_p, and E_p values for a bare Pt, a bare Au, and up to 10 CV cycles of Au deposited Pt electrodes.

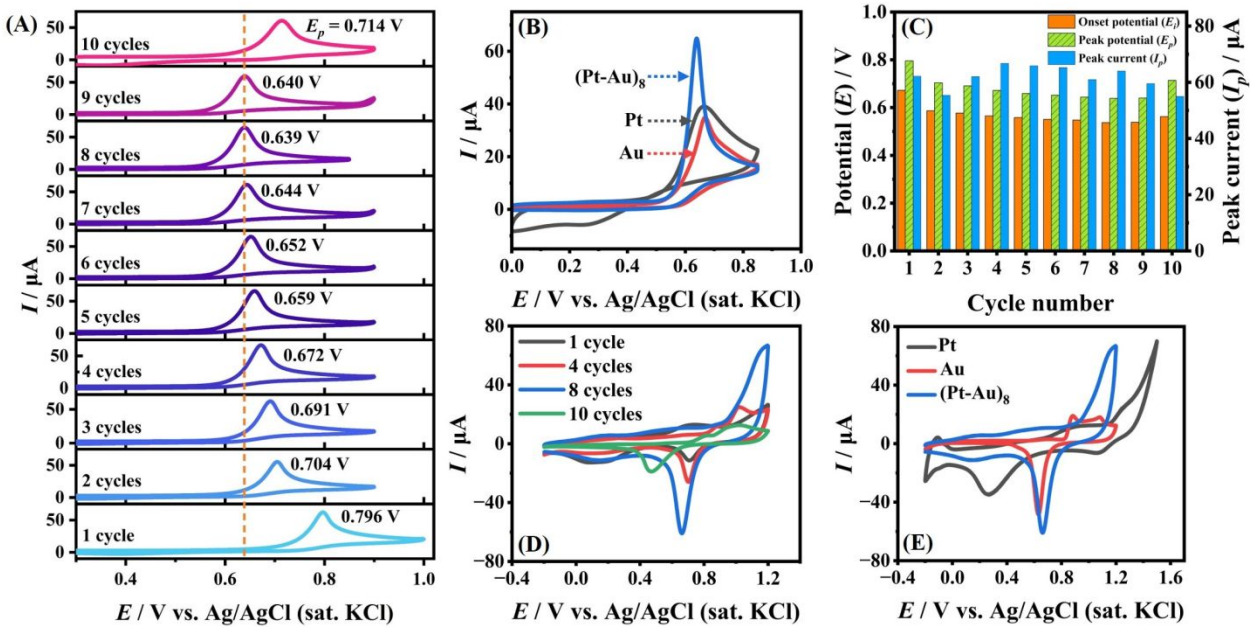

Figure 1. (A) Comparison of cyclic voltammograms (CVs) showing the performance of 1 to 10 CV cycles of Au deposition in attaining As(III) oxidation reaction. **(B)** Comparison of CVs among a bare Pt, a bare Au, and the $(Pt\text{-}Au)_8$ electrodes for As(III) oxidation reaction. **(C)** Bar chart demonstrating the trend in variation among onset potential (E_i), peak potential (E_p), and peak current (I_p) for various cycles numbers. The values in bar chart are derived from respective CVs in Figure 1A. **(D)** CVs recorded using Pt-Au electrode after varying Au deposition cycles on Pt in absence of arsenite solution. **(E)** Comparison among various characteristic CVs for a bare Pt, bare Au, and Au-modified Pt electrode in absence of arsenite solution. All the CVs were obtained at a scan rate of 0.1 Vs^{-1}. Arsenite oxidation performance of different electrodes were obtained by pipetting 200 µL of 0.1 M As(III) into a 10 mL 0.1 M H_2SO_4, achieving a final concentration of 2 mM As(III).

Anodic transfer coefficient (β) is a crucial kinetic parameter to comprehend various kinetic aspects. To determine β value, Tafel analysis was performed for a bare Au, a bare Pt, and 1 to 10 cycle Au deposited Pt electrodes based on **equation 1**.[28,29]

$$\log I = (\log I_0 - \frac{E^0}{b}) + \frac{E}{b} \quad (1)$$

Where, E^0 is the formal potential, E is the applied potential (vs. Ag/AgCl), I_0(=nFCk^0) is the exchange current at E=E^0, and b ($= \frac{2.3RT}{\beta F}$) is the Tafel slope. From the value of Tafel slope (b), anodic transfer coefficient (β) was determined and presented in **Table 1**. It can be clearly observed from **Table 1** that Pt-Au electrode with 8 deposition cycles of Au has the lowest Tafel slope value suggesting the least energy requirement for 10 times elevation of current with the $(Pt\text{-}Au)_8$ electrode. Now, turning to the anodic transfer coefficient (β), a β value below 0.5 signifies a concerted mechanistic pathway for the electrode process, while a β value above 0.5 points to a multistep charge transfer mechanism.[20,28,30] It can be seen in **Table 1** that the β value for As(III) oxidation reaction is lower than 0.5 for the pristine Au and Pt electrodes indicating concerted electron transfer mechanism during As(III) to As(V) oxidation, whereas the value is higher than 0.5 for Pt-Au electrodes implying that As(III) oxidation followed step wise electron transfer mechanism at the peak potential region. In the subsequent sections, further investigations were conducted to comprehend the probable phenomenon that might be occurring on the electrode surface during varying number of CV cycle Au deposition.

Table 1 Comparison of the performance of Pt electrodes modified with varying Au deposition cycles.

Electrodes	**Onset potential, E_i (V)**	**Peak potential, E_p (V)**	**Peak current, I_p (μA)**	**Tafel slope, b (mV dec^{-1})**	**Anodic transfer coefficient, β**
Bare Pt	0.5060	0.6660	39.11	161.3	0.3661
Bare Au	0.5080	0.6680	34.95	162	0.3645
$(Pt\text{-}Au)_1$	0.6725	0.7960	62.14	116	0.5091
$(Pt\text{-}Au)_2$	0.5867	0.7040	55.39	117	0.5047
$(Pt\text{-}Au)_3$	0.5773	0.6910	62.03	93	0.6350
$(Pt\text{-}Au)_4$	0.5653	0.6720	66.73	94	0.6282
$(Pt\text{-}Au)_5$	0.5587	0.6590	65.87	96	0.6151
$(Pt\text{-}Au)_6$	0.5507	0.6520	65.25	84	0.7030
$(Pt\text{-}Au)_7$	0.5480	0.6440	60.99	80	0.7381

$(Pt\text{-}Au)_8$	0.5374	0.6390	63.98	75.6	0.7811
$(Pt\text{-}Au)_9$	0.5387	0.6400	59.51	82	0.7201
$(Pt\text{-}Au)_{10}$	0.5626	0.7140	54.96	162	0.3645

N.B.: $(Pt\text{-}Au)_1$ to $(Pt\text{-}Au)_{10}$ denote successive electrodeposition of Au particles on Pt surface.

3.2. Electrochemical, morphological, and chemical characterization

3.2.1. Cyclic voltammetric characterization

Figure 1D illustrates the changes in CVs after each loading of Au particles on Pt electrode recorded in 0.1 M H_2SO_4 medium in absence of As(III) in the potential range $-0.2\ V < E_{Ag/AgCl} < +1.2\ V$. In the anodic scan, the peak around 1.0 V suggests the formation of gold oxide and hydroxide, which undergo reduction in the cathodic scan.[31] It can be observed that both anodic and cathodic peak current continuously increased for the electrodes prepared with 1 to 8 cycle deposition of Au film on the Pt surface. This indicates an increase in the electrochemically active sites on the Pt-Au electrode up to 8-cycle depositions. However, both the anodic and cathodic current substantially decreased in the characteristic CV obtained for Pt-Au electrode after 10 deposition cycles of Au on Pt, suggesting a huge drop in active surface area. Noticeable negative shift in cathodic peak potential for Au oxidation was observed after each successive deposition cycle. **Figure 1E** displays the characteristic CVs for a pristine Pt, Au, and the as-prepared Pt-Au electrode prepared with 8 cycles of Au deposition, also denoted as $(Pt\text{-}Au)_8$. A higher anodic and cathodic current is observed for the $(Pt\text{-}Au)_8$ electrode compared to the pristine polycrystalline Au electrode indicating a larger electroactive surface area for the Au modified Pt electrode. In contrast, the cathodic current for bare Pt electrode substantially decreased in case of the $(Pt\text{-}Au)_8$ electrode signifying the suppression of Pt-surface oxidation by the Au thin film on Pt surface.

3.2.2. Open circuit potential (OCP) analysis

Open circuit potential (OCP) is defined as the potential that exists in an open circuit. In other words, it is the voltage that exists when the terminal ends of a circuit are disconnected and there is no potential applied externally.[32] The intrinsic polarity that develops on an electrode surface is referred by the magnitude of OCP for that electrode. Therefore, in order to characterize the

electrode surface electrochemically, linear polarization curves were obtained for bare Au, bare Pt, and Au immobilized Pt electrodes in both the presence and absence of As(III) ions which are shown in **Figure 2**. **Figure 2A** exhibits the linear polarization curves for the three distinct electrodes in 0.1 M H_2SO_4 in absence of As(III). A pristine Au electrode has an OCP value of 0.24 V where the value is 0.43 V for a pristine Pt electrode, indicating that Pt has a more electron deficient positive surface than a bare Au electrode in acidic medium. Interestingly, the magnitude of OCP is much higher for the $(Pt\text{-}Au)_8$ electrode than the bare Pt and the bare Au electrodes having a value of 0.60 V.

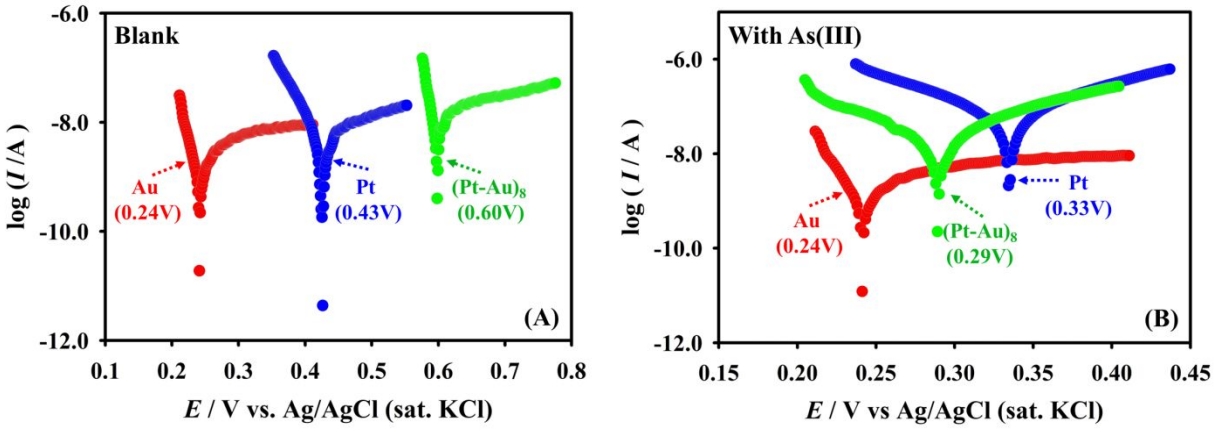

Figure 2. Linear Polarization curves recorded for **(A)** without As(III) and **(B)** with 2 mM As(III) prepared in 0.1 M H_2SO_4 solution recorded using bare Pt, bare Au, and $(Pt\text{-}Au)_8$ electrodes.

Linear polarization curves were recorded again in presence of As(III) ions in the acidic solution as shown in **Figure 2B**. Although, no shift was observed in case of bare Au electrode, the Pt electrode shifted negatively by about 0.10 V. On the contrary, the $(Pt\text{-}Au)_8$ electrode exhibited the greatest negative shifting by nearly 0.19 V. Since As(III) ions actually exist as negatively charged arsenite ions (AsO_2^-) in the medium,[33] the adsorption of these ions causes the OCP value to shift negatively. A higher negative shifting in case of Au modified Pt electrode can be accounted for the larger loading of the arsenite ions (AsO_2^-) on the most electron deficient $(Pt\text{-}Au)_8$ surface as projected in **Figure 2A**, relative to the bare Pt and Au surfaces. A competitive pre-adsorption step later facilitates the As(III) oxidation reaction which results in a higher oxidation current as shown in **Figure 1A** and **1C**.

3.2.3. Morphological characterization

Figure 3 exhibits the varying morphology and structure of Au particles on Pt surface with each successive CV cycle deposition. The Au deposition on Pt was obtained by cycling the potential between 0 to −1 V immersing the Pt electrode in 0.05 M $HAuCl_4$ aqueous solution. A metallic surface of Pt with various dents on the surface can be observed in **Figure 3** before any Au deposition. When 2 cycles of Au were deposited, a thin Au film formed on the Pt surface. After 4 cycles of Au deposition, the evenly dispersed Au particles were detected. When the number of cycles was increased up to 6, various Au agglomerated particles larger than 2 μm were spotted. The largest particle size extending up to 10 μm in size was witnessed after 8 Au deposition cycles.

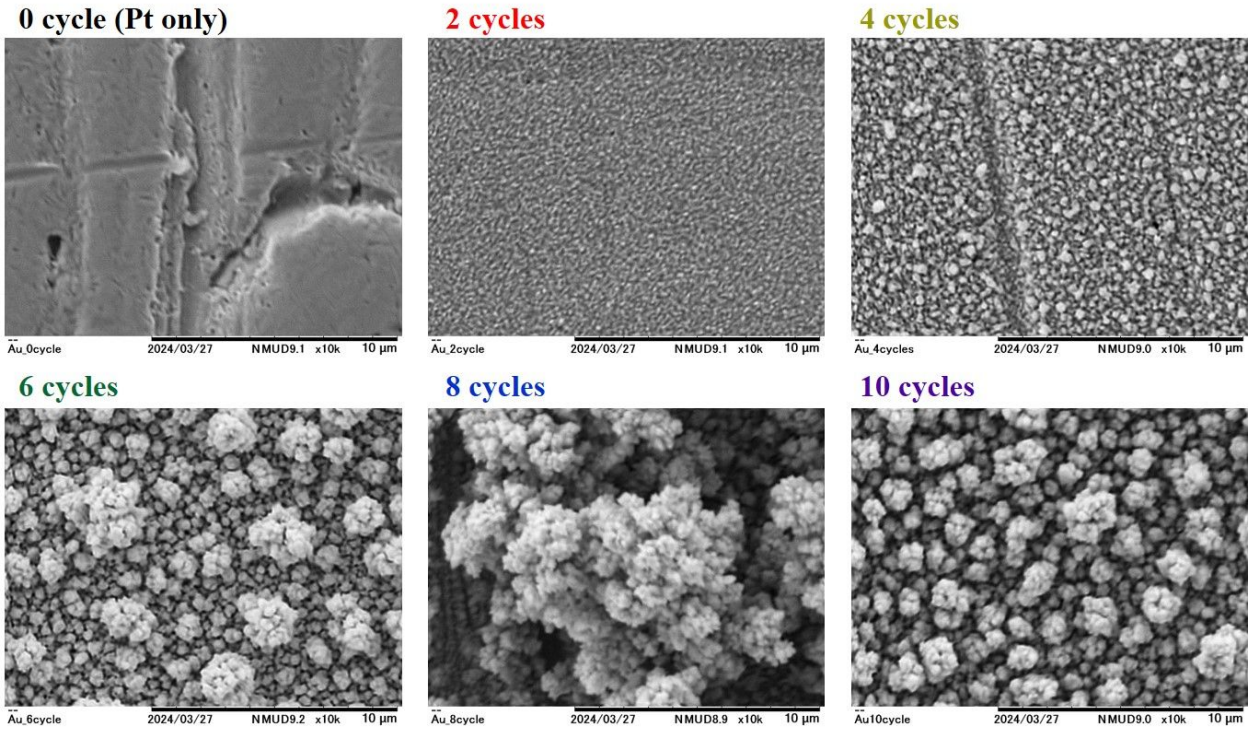

Figure 3. Scanning electron microscopy (SEM) images showing the variation in surface morphology after diverse Au deposition cycles on Pt surface. All the SEM images were taken at 10,000 times magnification of Pt-Au surfaces.

Surprisingly, the Au particles size suddenly dropped at the 10th deposition cycle. Hence, it is discernible that the highest loading of Au particles was obtained at the 8th deposition cycle which perhaps were able to assist in favorable pre-adsorption step of AsO^{2-} ions on the Pt-Au surface resulting in a higher oxidation current.[34]

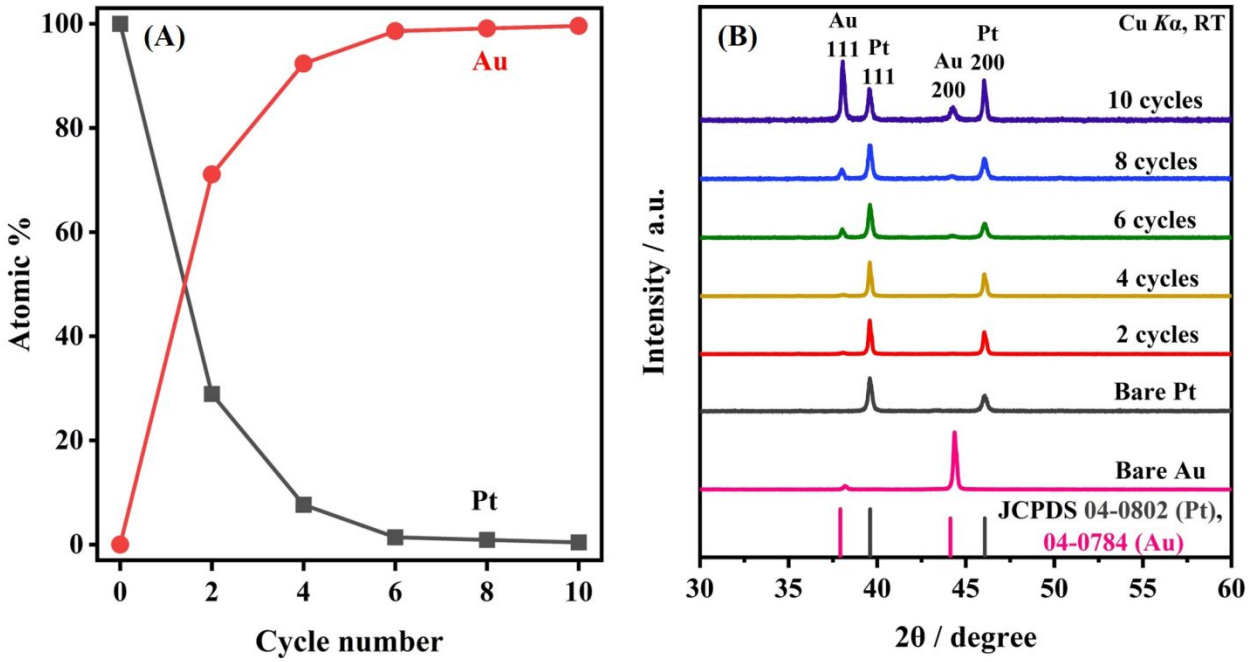

Figure 4. (A) Energy dispersive X-ray (EDX) data showing variation in the Au and Pt atomic % with increasing deposition cycle number. **(B)** X-ray diffraction (XRD) patterns showing the change in crystal structures of deposited Au layers on Pt surface with increasing deposition cycles.

The plot of energy dispersive X-ray (EDX) data in **Figure 4A** shows that the atomic % of Pt decreases while the atomic % of Au increases with each consecutive cycle. This indicates that the deposition of Au is progressively covering the surface of the Pt substrate. Additionally, the atomic ratio of Au becomes 98.6% and 99.11% saturated after 6 and 8 cycles of deposition, respectively. The atomic % of Au shows minimal increase after 6 cycles of deposition. Next, the XRD patterns in **Figure 4B** shows the successive growth of Au(111), Au(200), Pt(111), and Pt(200) crystal facets with increasing deposition cycles. The peak positions for both Au and Pt are consistent with the standard data (JCPDS 04-0802 for Pt and 04-0784 for Au). An increase in suitable facet intensity is beneficial as it can improve the overall catalytic performance of the Pt-

Au electrode by providing more active sites for the As(III) oxidation reaction.[26,27,35,36] Au(111) is the most stable and widely studied facet of Au, which has a smooth, close-packed surface that provides high stability, good adsorption, and catalytic properties.[37–40] Similar to Au(111), Pt(111) is also active for many catalytic reactions.[41,42] Hence, growth of Au(111) facets coupled with existing Pt(111) facets provides good adsorption and catalytic oxidation of As(III) species. Thus, it is expected that an increase in the intensity of Au(111) XRD peak would be beneficial for a more efficient electrode performance by providing more active site on the Pt-Au surface. However, the growth of comparatively less stable Au(200) facet possibly have declined the performance of Pt-Au electrode after 10 cycles of Au deposition.[38,43,44] This also explains why bare Au exhibit less adsorptive and catalytic performance which is predominantly oriented to Au(200), as described in **Figure 1B**, **Figure 2**, and **Figure 4B**. Particularly, the linear polarization curves in **Figure 2B** support the finding that the Au(111) facets of the $(Pt\text{-}Au)_8$ electrode facilitate the adsorption of As(III) ions, compared to the relatively inactive Au(200) facets of the pristine polycrystalline gold electrode. Notably, the Pt(200) facets have also started to dominate Pt(111) at the 10^{th} cycle of Au deposition in comparison to the rest of the cycle numbers, which presumably have also dropped the catalytic efficiency of the Pt-Au electrode. Moreover, to gain insight into the growth of Au crystallite size and potential changes in lattice parameters, Le Bail fitting was performed (shown in **Table 2**). The lattice constants of both Au and Pt were found to remain nearly unchanged across all samples, while the crystallite size was observed to increase from 2 to 6 cycles, then saturated from 6 to 10 cycles. This behavior aligns with the saturation of the Au atomic ratio from 6-cycle depositions, as revealed by EDX analysis **Figure 4A**.

Table 2 Space group, lattice constant and crystallite size of Au particles on Pt.

Cycle Number	Au			Pt	
	Space group	Lattice constant / Å	Crystallite size / nm	Space group	Lattice constant / Å
0 cycle	Fm-3m	-	-	Fm-3m	3.94101(8)
2 cycles	Fm-3m	4.0920(7)	29(2)	Fm-3m	3.94097(5)
4 cycles	Fm-3m	4.0921(7)	37(2)	Fm-3m	3.94101(5)
6 cycles	Fm-3m	4.0937(2)	63(3)	Fm-3m	3.94112(8)
8 cycles	Fm-3m	4.0948(3)	61(2)	Fm-3m	3.94130(9)

10 cycles	Fm-3m	4.0936(1)	69(2)	Fm-3m	3.94141(1)

3.2.4. X-ray photoelectron spectroscopy analysis

X-ray photoelectron spectroscopy (XPS) is a preferable technique to comprehend the chemical states of an electrode surface. The deposited Au layer on Pt surface was studied employing XPS technique as illustrated in **Figure 5**. The two peaks appearing at around 84.21 eV and 87.88 eV are generally assigned to Au $4f_{7/2}$ and Au $4f_{5/2}$, respectively.[45,46] The existence of these two peaks for all XPS spectrum of Au 4f indicates that Au was deposited in its zero valent metallic form for all electrodes with their varying Au deposition cycles.[47] Notably, the binding energies decreased consecutively for both peaks, but they increased suddenly for the 10^{th} cycle of Au deposition subtly. This red shift in binding energies during the first 8-cycle suggests an interfacial interaction between Au and Pt, with Au surfaces receiving electron density from Pt, thereby lowering the binding energies for the Pt-Au electrodes. Interestingly, a blue shift in binding energies is observed starting from the 8^{th} Au deposition cycle, indicating a threshold for optimal interfacial interaction.

XPS peak separation unveils vital information about electronic environment of atoms. The ideal peak separation between Au $4f_{7/2}$ and Au $4f_{5/2}$ for a pure metallic Au surface was estimated to be 3.67 eV.[45,46] A shift in peak separation can be caused by a change in electronic environment around the atoms.[48] The deposition of 8 cycles of Au on the Pt surface resulted in the highest peak separation of 3.69 eV, likely attributable to intermetallic interactions between Au atoms and the underlying Pt substrate. This synergistic effect enhanced the electrode's performance as an efficient catalyst for the oxidation of As(III). Notably, the separation between the two characteristic peaks for metallic Au dropped to 3.67 eV for 10 cycles of Au deposition implying that the Au particles on $(Pt\text{-}Au)_{10}$ surface has begun to act like bulk Au atoms having no interaction with the Pt substrate. The similarity in Tafel slope values between the $(Pt\text{-}Au)_{10}$ electrode and the bare gold electrode (as shown in **Table 1**) for the As(III) oxidation reaction further supports the conclusion that Au particles at 10-cycle depositions on Pt follow an electron transfer kinetics comparable to bare Au.

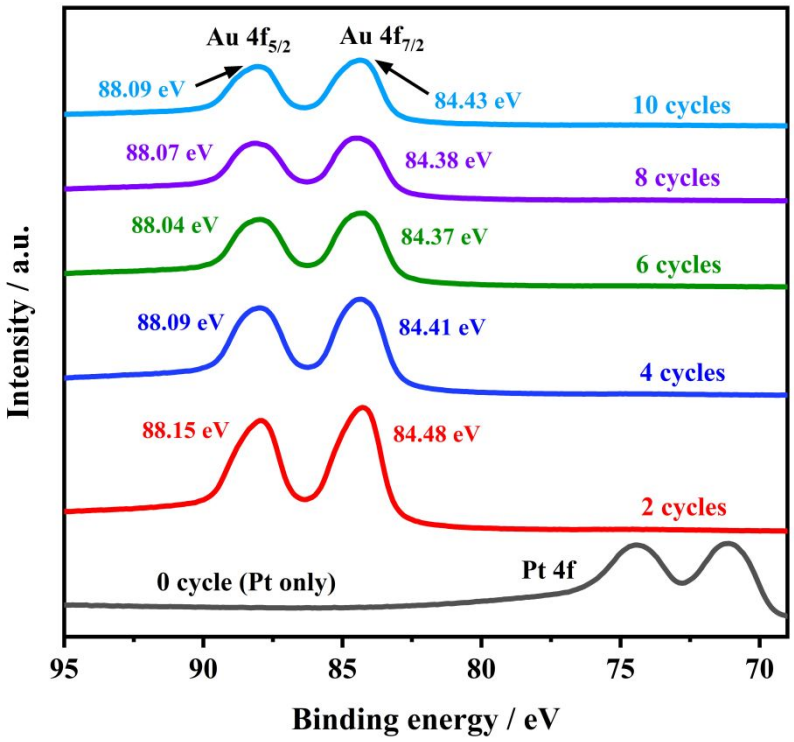

Figure 5. X-ray photoelectron spectroscopy (XPS) spectrum of a bare Pt and Pt-Au electrodes recorded after various cycles of Au deposition.

The preceding discussion has substantiated the catalytic, morphological, and chemical efficiency of the $(Pt\text{-}Au)_8$ electrode, therefore, further kinetic investigation was conducted using this electrode.

3.3. Kinetics

3.3.1. Effect of As(III) concentration

Figure 6A shows the development of CV profiles with increasing As(III) concentration in the reaction medium. The CV peak potentials were found to vary from 0.75 V to 0.80 V as the concentration was elevated from 0.2 mM to 4.0 mM As(III). This event implies that the $(Pt\text{-}Au)_8$ electrode requires concentration overpotential for oxidizing As(III) with rising concentration. The correlation between CV peak current (I_p) and As(III) concentration is depicted in **Figure 6B**. The figure shows excellent correlation between I_p and As(III) concentration with a regression coefficient (R^2) value of 0.99. To unveil the kinetic order of As(III) oxidation reaction, log(I) vs. log[As(III)] graph was plotted at three different potentials (0.810 V, 0.815 V, and 0.820 V)

retrieved from the mass-transfer limited regions of the CVs. With the assumption that the log (*I*) vs. log [As(III)] curve yields a straight line, the value of m can be calculated from the dependence of currents on the concentration of the electro-active species, as shown by **equation 2**.[49]

$$\log I = \log k + m \log [\text{As(III)}] \quad (2)$$

Where, *m* is the order of reaction and *k* is the reaction rate constant. The slopes of three regression lines shown in **Figure 6C** were calculated using e**quation 2**. The results were 1.21, 1.18 and 1.14 for 0.810 V, 0.815 V, and 0.820 V, respectively, which are very close to 1, indicating that the As(III) oxidation reaction followed first order kinetics on $(Pt\text{-}Au)_8$ electrode surface. A first-order kinetics implies that the rate of As(III) oxidation reaction on $(Pt\text{-}Au)_8$ electrode surface is directly proportional to the concentration of As(III) in the bulk of the reaction medium.[50]

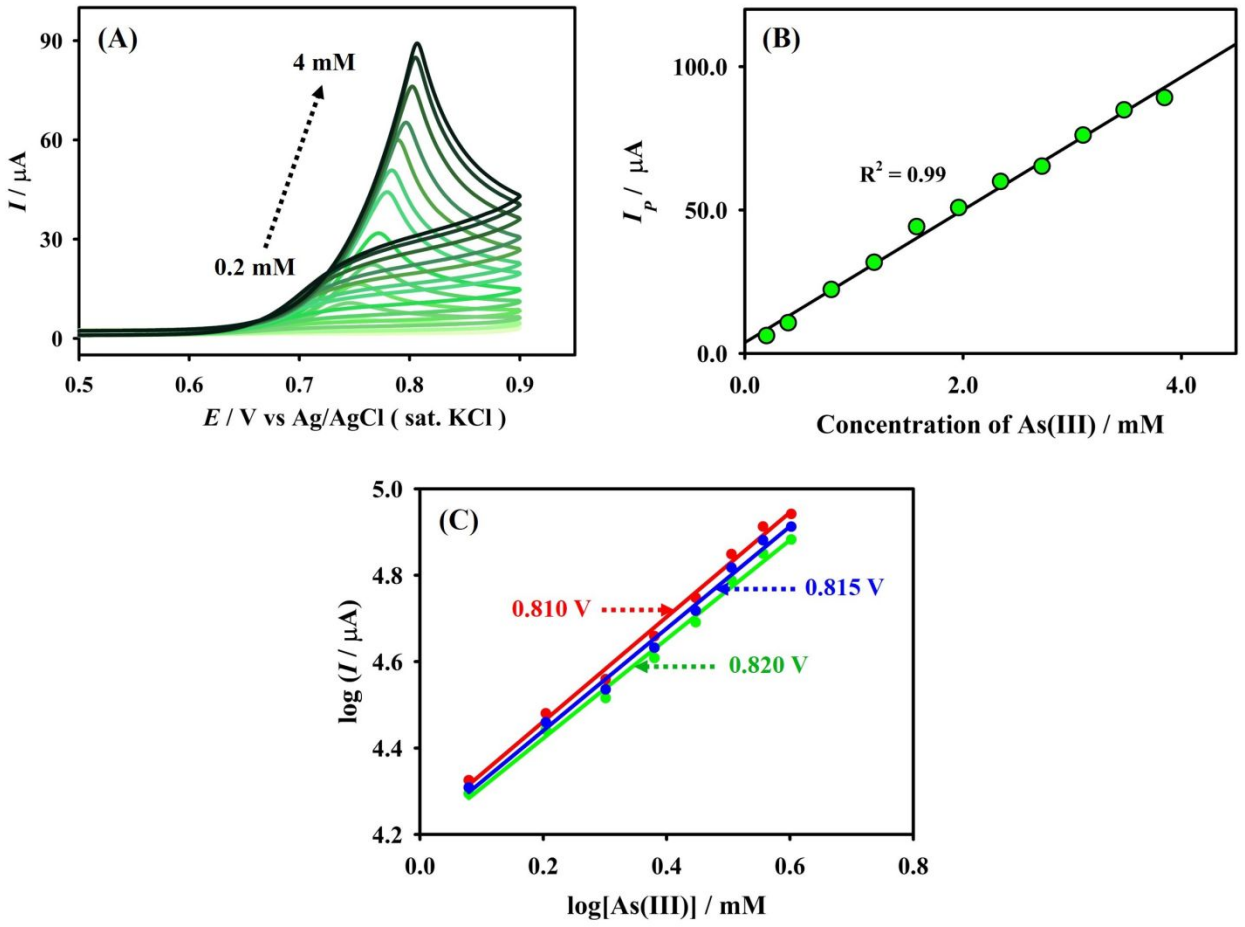

Figure 6. (A) Variation of CVs with As(III) concentration recorded using $(Pt\text{-}Au)_8$ electrode in 0.1 M H_2SO_4 at a scan rate of 0.1 Vs^{-1}. **(B)** Calibration curve showing the dependence of peak current (I_p) on As(III) concentration. **(C)** log (I) vs. log[As(III)] plot for three different potentials. The data in Figure 6B and 6C were extracted from Figure 6A.

3.3.2. Effect of scan rate

A key trait of a highly active electrode is its proficiency in sustaining faradaic processes even at elevated scan rates. This proficiency is due to the decreased thickness of the diffusion layer as the scan rate rises, which enhances the mass transfer rate.[32] Such an electrode can uphold the faradaic charge-transfer electrochemical process despite having numerous masses on its surface, thereby achieving a higher current density. Conversely, a less active electrode is restricted by its reaction rate, resulting in a lower current density. To discover various crucial kinetic parameters associated with As(III) oxidation on the $(Pt\text{-}Au)_8$ surface, CVs were recorded for As(III) oxidation at scan rates varying from 0.025 to 0.4 Vs^{-1} as shown in **Figure 7A**. To unveil the mass transfer character during As(III) oxidation, log (I_p) was plotted against log of scan rates as displayed in **Figure 7C**. The theoretical slope value for the plot of log (I_p) versus log (v) is 0.5 for an ideal diffusion-controlled process, whereas it is 1 for a process entirely limited by adsorption kinetics. [32,51,52] In the present case, the slope was found to be 0.44, which is in close proximity to 5, therefore, it can be inferred that the As(III) oxidation kinetics was limited by diffusion of As(III) ions to the $(Pt\text{-}Au)_8$ electrode surface. Furthermore, the positive shifting of peak potential (E_p) with varying scan rates in **Figure 7B** also supports the diffusion-limited kinetics of As(III) oxidation on the proposed electrode.[53,54] This diffusion-limited process, coupled with first-order kinetics, is highly desirable for an electrochemical sensor as it prevents electrode surface fouling and deactivation due to product accumulation, while ensuring a steady supply of reactants.

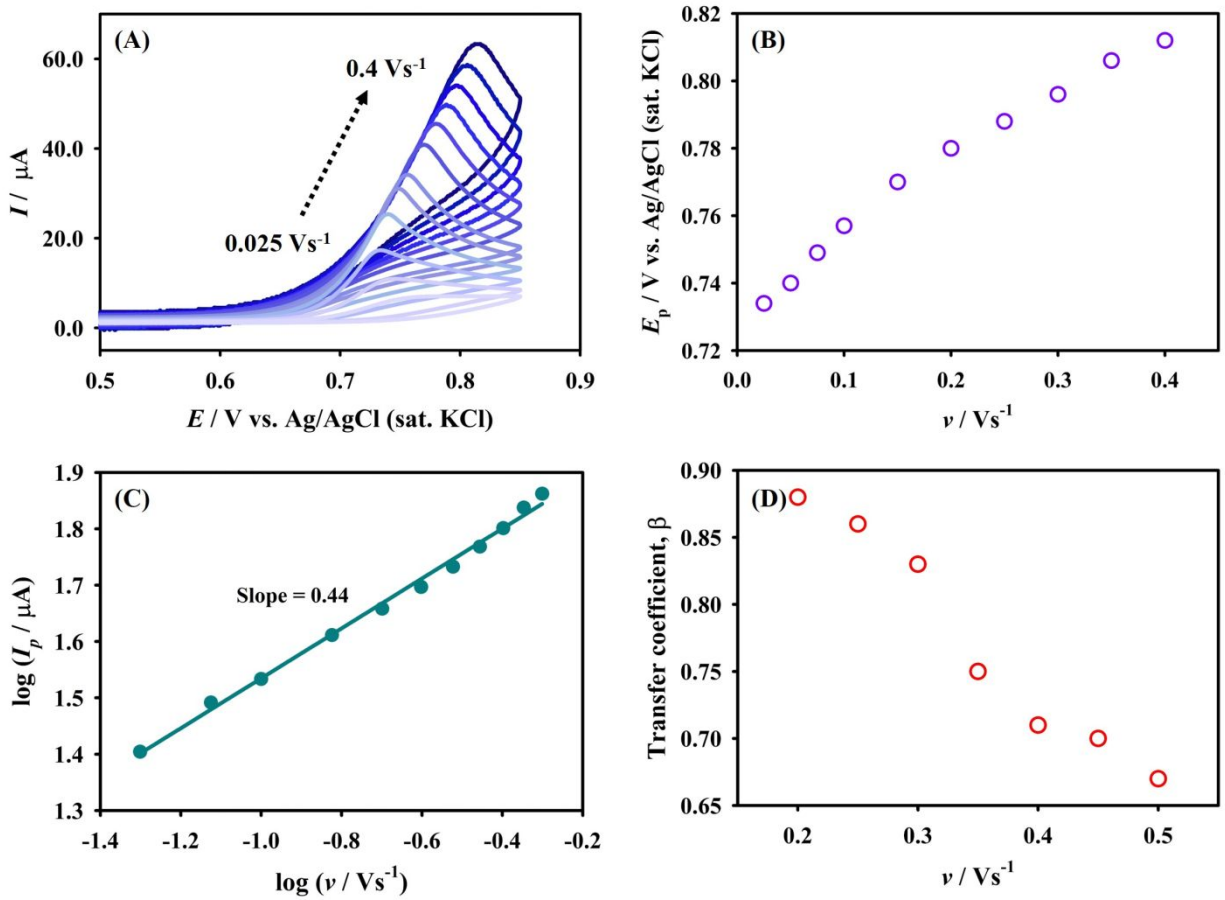

Figure 7. (A) CVs of As(III) oxidation recorded using $(Pt\text{-}Au)_8$ electrode for 2 mM As(III) prepared in 0.1 M H_2SO_4 solution at variable scan rates (from 0.025 to 0.4 Vs^{-1}). **(B)** Variation of peak potential (E_p) with change in scan rate (v). **(C)** Variation of logarithm of I_p with logarithm of v. **(D)** Variation of anodic transfer coefficient (β) with changing scan rate.

Next, the transfer coefficients for the anodic process (β) was calculated using the following **equation 3**.[32,55]

$$\beta = \frac{1.86RT}{F|E_p - E_{p/2}|} \quad (3)$$

Where, F = 96485 C mol^{-1} is the Faraday constant and $E_{p/2}$ is the half-peak potential. It can be observed from **Figure 7D** that the magnitude of β varied substantially with variable scan rates and they exceed 0.5 in all cases. Previously in section 3.1., we estimated the β value to be 0.78 for $(Pt\text{-}Au)_8$ electrode using the Tafel **equation 1** in the kinetic region of CV. Now, we also acquired an average β value of 0.77 in the mass-transfer regions of CVs for variable scan rates.

Thus, it can be inferred that As(III) oxidation reaction followed stepwise mechanistic pathway in both kinetic and mass-transfer regions of CV on $(Pt\text{-}Au)_8$ electrode surface. Therefore, the overall stepwise electron transfer reaction pathway for the arsenite to arsenate oxidation reaction, involving a pre-adsorption step, is presented in **equation 4**.[56]

$$As^{(III)}O_2^- \xrightarrow{Adsorption} (As^{(III)}O_2^-)_{ads} \xrightarrow{-1e^-} [As^{(IV)}O_2^-]^* \xrightarrow[H_2O]{-1e^-} As^{(V)}O_4^{3-} \quad (4)$$

3.4. Sensing activities

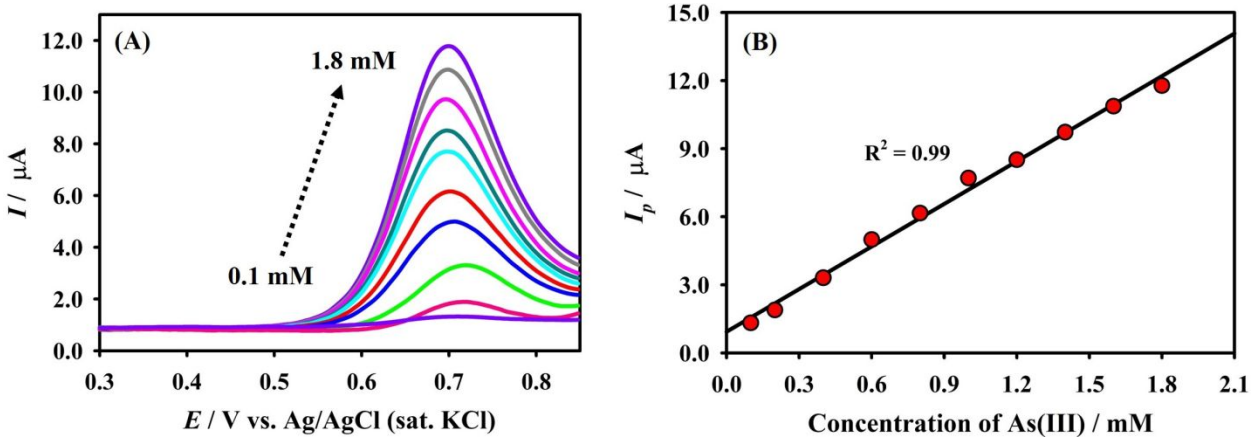

Figure 8. (A) Differential pulse voltammograms (DPVs) for As(III) oxidation reaction obtained using $(Pt\text{-}Au)_8$ electrode in 0.1 M H_2SO_4 with pulse amplitude, pulse width, and pulse period of 0.05 V, 0.05 sec, and 0.5 sec, respectively. **(B)** Calibration curve exploited from DPVs showing the correlation between I_p and As(III) concentration.

The sensing performance of the proposed $(Pt\text{-}Au)_8$ electrode was checked using the differential pulse voltammetry method within the As(III) concentration range 0.1 mM to 1.8 mM, as displayed in **Figure 8A**. The calibration curve shown in **Figure 8B** is a crucial plot for estimating various important sensor parameters. The DPV peak currents exhibited a linear relation with As(III) concentration as substantiated by the linear regression coefficient value of 0.99. From the calibration curve, the limit of detection (LOD) for As(III) detection was determined using **equation 5** which was found to be 65.39 µM with a signal-to-noise ratio (S/N) of 3. The sensitivity value of the $(Pt\text{-}Au)_8$ electrode for As(III) detection was measured to be 23.13 µA mM^{-1}.

$$LOD = \frac{3 \times SD}{SR} \quad (5)$$

Where *SD* denotes the standard deviation of current values within As(III) oxidation potential range found for three blank response and *SR* stands for slope of the regression line shown in **Figure 8B**. **Table 3** presents various previously reported analogues for As(III) detection from the literature, highlighting the superior performance of the developed electrode, which achieves the lowest potential while maintaining a broad linearity range.

Table 3 Overview of the several previously reported analogous electrodes for arsenite oxidation.

Electrode	Technique	Electrolyte	Peak potential, $E_{p(Ag/AgCl)}$ / V	LDR / µM	LOD	Ref.
Pt/GCE	LSV	1 M $HClO_4$	0.89	1–50	0.028 µM	[57]
Pt_{nano}/BDD	SWASV	0.1 M H_2SO_4	0.88	1.3–13.34	0.5 ppb	[58]
Pt–Pd	SWV	0.1 M H_2SO_4	0.82	5-225	1.3 ppb	[19]
Au	CV	0.1 M PBS (pH=3)	0.72	100-1000	-	[21]
$(Pt\text{-}Au)_8$	DPV	0.1 M H_2SO_4	0.70	100-1800	65.39 µM	This work

Abbreviations: LDR- Linear dynamic range, **LOD-** Limit of detection, **GCE-** Glassy carbon electrode, **LSV-** Linear sweep voltammetry, **BDD-** Boron doped diamond, **SWASV**- Square wave anodic striping voltammetry, **SWV-** Square wave voltammetry, **CV-** Cyclic voltammetry, **PBS-** Phosphate buffer solution, **DPV-** Differential pulse voltammetry.

Good stability is another essential criterion of an ideal sensor. Chronoamperometric technique was employed at 0.70 V vs. Ag/AgCl (sat. KCl) for 600 seconds to evaluate the stability of the electrode's performance, as shown in **Figure 9A**. Batch injection method was adopted during the process, where 100 µL of 0.1 M As(III) solution was injected in every 30-second intervals onto the surface of the $(Pt\text{-}Au)_8$ electrode. A faradic current with a magnitude of about 1 mA spiked sharply following each injection, which rapidly dropped to baseline due to the diffusion of As(III) species away from the electrode surface. Interestingly, the current spikes for all the

injections are significantly identical underscoring the remarkable stability and repeatability of the electrode for detecting arsenite species. The stability of the proposed sensor was further investigated by conducting 500 CV cycling with the $(Pt\text{-}Au)_8$ electrode in presence of 2 mM As (III) solution. The outcome displayed in **Figure S1** demonstrates no significant change in onset potential (E_i), peak potential (E_p), and peak current (I_p) ever after 500 cycles of CV runs boasting an impressive stability of the proposed electrode.

In real water samples, interference in electrochemical sensing may arise from various commonly co-existing ionic species. Therefore, salt solutions containing Na^+, NO_3^-, Cu^{2+}, SO_4^{2-}, Fe^{2+}, Fe^{3+}, Cl^-, CO_3^{2-}, NH_4^+, Ca^{2+}, and HCO_3^-, each at concentrations 10 times higher than As(III), were tested for potential interference by injecting them at 30-second intervals, as shown in **Figure 9B**. No noteworthy current response was observed from most of the ions at 0.70 V, demonstrating exceptional selectivity of the proposed electrode for As(III) species. Intriguingly, the electrode surface remained unaffected despite the addition of concentrated potential interfering compounds, and the current response associated with arsenite oxidation persisted at the end for three consecutive injections. It is worth noting that potential interference was observed from Fe^{2+} oxidation, but this can be disregarded in real samples, as Fe^{2+} is readily oxidized to Fe^{3+} by air. Fe^{3+} did not cause any interference with the developed electrode, as shown in **Figure 9B**.

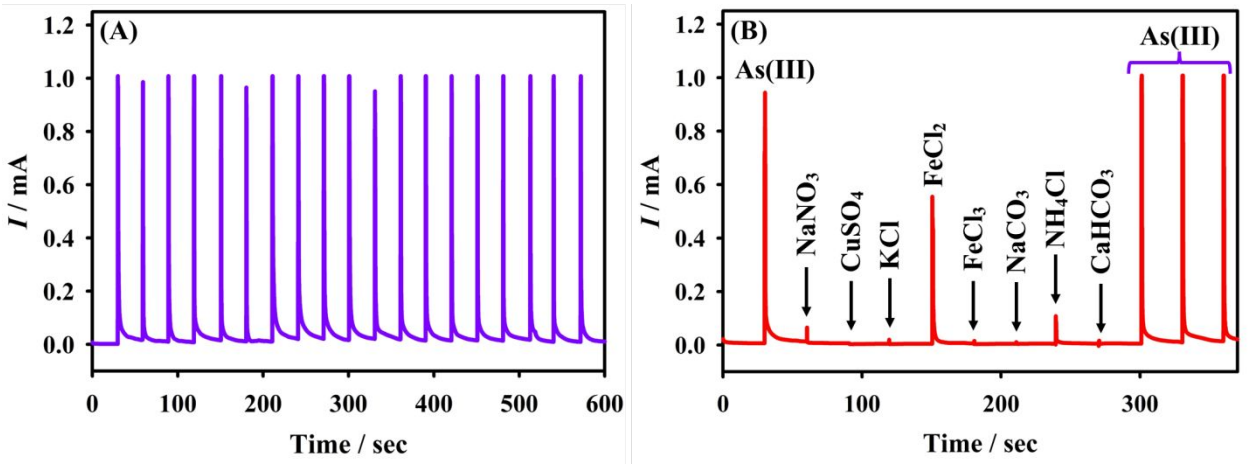

Figure 9. (A) Chronoamperometric *i-t* curve recorded by consecutive injection of 100 µL of 0.1 M As(III) onto the $(Pt\text{-}Au)_8$ electrode, demonstrating the stable current output over an extended period. **(B)** *i-t* curve recorded to evaluate interference from commonly co-existing ions by

injecting 100 μL of 1.0 M solutions (10 times more concentrated than As(III)). Injections were performed in batch mode at 30-second intervals, with a fixed potential of 0.70 V.

To demonstrate the practicality of the proposed electrode for detecting As(III) in real-world conditions, groundwater samples were collected from four different districts in Bangladesh, as presented in **Table 4**. The analysis was carried out using the linear sweep voltammetry (LSV) method, with 1 mM As(III) solutions prepared as described in **Text S2**. **Figure S2** showcases representative LSVs for the real samples, revealing a positive shift in the oxidative peak potential (E_p), likely due to the reducing nature of the groundwater. Exceptional recoveries, ranging from 97% to 108%, as shown in **Table 4**, endorse the electrode's reliability and potential for real-life applications.

Table 4 Statistical quantification of As(III) detection by $(Pt\text{-}Au)_8$ electrode in real samples.

Groundwater source	**Added concentration / mM**	**Obtained concentration[a] / mM**	**RSD[b] (%)**	**Recovery[c] (%)**
Feni	1.0	1.04	0.09	104
Jashore	1.0	0.971	2.52	97.1
Panchagarh	1.0	1.0	0.05	100
Sylhet	1.0	1.08	0.17	108

[a] Average of the three repeated As(III) measurements following LSV method obtained using $(Pt\text{-}Au)_8$ electrode. [b] Relative standard deviation (RSD) value represents the precision of the three measurements. [c] Recovery % = (obtained concentration ÷ added concentration)×100.

4. Conclusion

This study explored the optimal sensing performance for Au modified Pt electrode for arsenite oxidation, unveiling the physical and chemical factors driving this enhanced performance. The novel Pt-Au electrode was created by cathodic electrodeposition of Au particles sourced from

$HAuCl_4$ onto a Pt disc electrode. The Pt-Au electrode exhibited superior performance for arsenite oxidation compared to both pristine Au and Pt electrodes. Afterwards, optimization of Au deposition cycles, explored with CV, SEM, EDX, XRD, and XPS analysis, revealed that Pt-Au electrode exhibits best catalytic performance with 8 cycles of Au deposition owing to the optimal synergism between the deposited Au and the Pt substrate. Additionally, the optimal growth of Au(111) and Pt(111) crystal facets occurs at the 8^{th} Au deposition cycle, facilitating the pre-adsorption of arsenite ions on the Pt-Au electrode for the subsequent As(III) oxidation reaction. Kinetic investigations through concentration and scan rate effects disclosed that As(III) oxidation followed a diffusion-limited mass-transfer character, following a first-order reaction with stepwise electron transfer kinetics on the $(Pt\text{-}Au)_8$ electrode surface. The sensitivity of As(III) electro-oxidation on $(Pt\text{-}Au)_8$ electrode was calculated to be 23.13 $\mu A\ mM^{-1}$ with an LOD of 65.39 μM for the linearity range 0.1 to 1.8 mM. The as-prepared electrode demonstrated excellent stability, hence, can be proposed for routine analysis of As(III) in acidic medium. The proposed electrode is also expected to exhibit similar catalytic activity trends for other analytes, such as ethanol oxidation, methanol oxidation, and peroxide oxidation, which are our ongoing focus of research.

Acknowledgement

The authors acknowledge the Researchers Supporting Project number (RSP2024R30), King Saud University, Riyadh, Saudi Arabia for funding this research work. Ministry of Education (Grant No. PS 20201512), Bangladesh and Shahjalal University of Science Technology research center (Grant No. PS/2023/1/02) are also acknowledged for a partial support. K.A. and Y.N. appreciated the support of JST CREST Grant No. JPMJCR21B3, Japan.

Author Contributions

Mohammad Imran Hossain: writing – original draft, data curation, formal analysis, investigation, software; **Surove Rani Saha:** writing – original draft (supporting), investigation, data curation, formal analysis; **Kentaro Aoki:** writing – review & editing, material characterization, software; **Md. Mahfujul Alam:** writing – review & editing; **Nayan Ranjan Singha:** writing – review & editing; **Mostafizur Rahaman:** writing – review & editing, funding

acquisition; **Ali Aldalbahi:** writing – review & editing, funding acquisition; **Yuki Nagao:** material characterization, funding acquisition, resources for material characterization; **Mohammad A. Hasnat:** conceptualization, visualization, methodology, resources, funding acquisition, project administration, supervision.

Conflict of Interest

The authors have no financial/commercial conflicts of interest to declare.

References

1 D. Panagiotaras, G. Panagopoulos, D. Papoulis and P. Avramidis, Arsenic geochemistry in groundwater system, *Geochemistry-Earth's Syst. Process.*, 2012, 27–38.

2 Z. Rahman and V. P. Singh, The relative impact of toxic heavy metals (THMs)(arsenic (As), cadmium (Cd), chromium (Cr)(VI), mercury (Hg), and lead (Pb)) on the total environment: an overview, *Environ. Monit. Assess.*, 2019, **191**, 1–21.

3 J. F. Rivera, I. Pignot-Paintrand, E. Pereira, B. L. Rivas and J.-C. Moutet, Electrosynthesized iridium oxide-polymer nanocomposite thin films for electrocatalytic oxidation of arsenic (III), *Electrochim. Acta*, 2013, **110**, 465–473.

4 N. R. Council, *Arsenic in drinking water*, National Academies Press, 1999.

5 K. J. Whaley-Martin, B. J. Mailloux, A. van Geen, B. C. Bostick, K. M. Ahmed, I. Choudhury and G. F. Slater, Human and livestock waste as a reduced carbon source contributing to the release of arsenic to shallow Bangladesh groundwater, *Sci. Total Environ.*, 2017, **595**, 63–71.

6 M. M. Rahman, M. Asaduzzaman and R. Naidu, Consumption of arsenic and other elements from vegetables and drinking water from an arsenic-contaminated area of Bangladesh, *J. Hazard. Mater.*, 2013, **262**, 1056–1063.

7 M. I. Hossain, A. Bukhari, H. Almujibah, M. M. Alam, M. N. Islam, T. A. Chowdhury, S. Islam, M. Joardar, T. Roychowdhury and M. A. Hasnat, Validation of the efficiency of

arsenic mitigation strategies in southwestern region of Bangladesh and development of a cost-effective adsorbent to mitigate arsenic levels, *J. Environ. Manage.*, 2023, **348**, 119381.

8 B. K. Mandal, Y. Ogra and K. T. Suzuki, Identification of dimethylarsinous and monomethylarsonous acids in human urine of the arsenic-affected areas in West Bengal, India, *Chem. Res. Toxicol.*, 2001, **14**, 371–378.

9 N. Yogarajah and S. S. H. Tsai, Detection of trace arsenic in drinking water: challenges and opportunities for microfluidics, *Environ. Sci. Water Res. Technol.*, 2015, **1**, 426–447.

10 H. Yu, C. Li, Y. Tian and X. Jiang, Recent developments in determination and speciation of arsenic in environmental and biological samples by atomic spectrometry, *Microchem. J.*, 2020, **152**, 104312.

11 D. Sanchez-Rodas, W. T. Corns, B. Chen and P. B. Stockwell, Atomic fluorescence spectrometry: a suitable detection technique in speciation studies for arsenic, selenium, antimony and mercury, *J. Anal. At. Spectrom.*, 2010, **25**, 933–946.

12 Z. H. Khan, M. H. Ullah, B. Rahman, A. I. Talukder, M. Wahadoszamen, K. M. Abedin and A. Haider, Laser-Induced Breakdown Spectroscopy (LIBS) for Trace Element Detection: A Review, *J. Spectrosc.*, 2022, **2022**, 3887038.

13 M. Wang, J. He, J. Luo, J. Hu and X. Hou, Ultrasensitive determination and non-chromatographic speciation of inorganic arsenic in foods and water by photochemical vapor generation-ICPMS using CdS/MIL-100 (Fe) as adsorbent and photocatalyst, *Food Chem.*, 2022, **375**, 131841.

14 F. Ardini, G. Dan and M. Grotti, Arsenic speciation analysis of environmental samples, *J. Anal. At. Spectrom.*, 2020, **35**, 215–237.

15 M. S. Reid, K. S. Hoy, J. R. M. Schofield, J. S. Uppal, Y. Lin, X. Lu, H. Peng and X. C. Le, Arsenic speciation analysis: A review with an emphasis on chromatographic separations, *TrAC Trends Anal. Chem.*, 2020, **123**, 115770.

16 H. Hu, B. Xie, Y. Lu and J. Zhu, Advances in Electrochemical Detection Electrodes for As (III), *Nanomaterials*, 2022, **12**, 781.

17 L. Pujol, D. Evrard, K. Groenen-Serrano, M. Freyssinier, A. Ruffien-Cizsak and P. Gros, Electrochemical sensors and devices for heavy metals assay in water: the French groups' contribution, *Front. Chem.*, 2014, **2**, 19.

18 M. Bhattu, M. Verma and D. Kathuria, *Recent advancements in the detection of organophosphate pesticides: A review*, 2021, vol. 13.

19 M. M. Alam, M. A. Rashed, M. M. Rahman, M. M. Rahman, Y. Nagao and M. A. Hasnat, Electrochemical oxidation of As (III) on Pd immobilized Pt surface: kinetics and sensing performance, *RSC Adv.*, 2018, **8**, 8071–8079.

20 M. Ahsan, M. M. Rahman, A. E. Alsafrani, M. A. Aziz, A. Almahri, H. M. Marwani, M. M. Rahman and M. A. Hasnat, Immobilization of poly (o-aminophenol) film on Pt surface: A robust sensor for detecting As (III) in an acidic medium, *Surfaces and Interfaces*, 2023, **39**, 102976.

21 M. Ahsan, M. Z. Bin Mukhlish, N. Khatun and M. A. Hasnat, pH dependent electro-oxidation of arsenite on gold surface: Relative kinetics and sensitivity, *Heliyon*, 2023, **9**, e14192.

22 Y. Liu, Z. Huang, Q. Xie, L. Sun, T. Gu, Z. Li, L. Bu, S. Yao, X. Tu and X. Luo, Electrodeposition of electroreduced graphene oxide-Au nanoparticles composite film at glassy carbon electrode for anodic stripping voltammetric analysis of trace arsenic (III), *Sensors Actuators B Chem.*, 2013, **188**, 894–901.

23 A. O. Idris, J. P. Mafa, N. Mabuba and O. A. Arotiba, Nanogold modified glassy carbon electrode for the electrochemical detection of arsenic in water, *Russ. J. Electrochem.*, 2017, **53**, 170–177.

24 J. M. Feliu and E. Herrero, Pt single crystal surfaces in electrochemistry and electrocatalysis, *EES Catal.*, 2023, **2**, 399–410.

25 A. Dutta, M. M. Hasan, M. R. Miah, Y. Nagao and M. A. Hasnat, Efficient sensing of hydrogen peroxide via electrocatalytic oxidation reactions using polycrystalline Au electrode modified with controlled thiol group immobilization, *Electrochim. Acta*, 2021, **395**, 139217.

26 M. R. Rahman, T. Okajima and T. Ohsaka, Selective Detection of As(III) at the Au(111)-like Polycrystalline Gold Electrode, *Anal. Chem.*, 2010, **82**, 9169–9176.

27 J. Lipkowski, Z. Shi, A. Chen, B. Pettinger and C. Bilger, Ionic adsorption at the Au(111) electrode, *Electrochim. Acta*, 1998, **43**, 2875–2888.

28 A. J. Bard, L. R. Faulkner and H. S. White, *Electrochemical methods: fundamentals and applications*, John Wiley & Sons, 2022.

29 M. F. Shabik, M. M. Hasan, K. A. Alamry, M. M. Rahman, Y. Nagao and M. A. Hasnat, Electrocatalytic oxidation of ammonia in the neutral medium using Cu2O.CuO film immobilized on glassy carbon surface, *J. Electroanal. Chem.*, 2021, **897**, 115592.

30 H.-H. Yang and R. L. McCreery, Elucidation of the Mechanism of Dioxygen Reduction on Metal-Free Carbon Electrodes, *J. Electrochem. Soc.*, 2000, **147**, 3420.

31 N. Hassan and R. Holze, A comparative electrochemical study of electrosorbed 2- and 4-mercaptopyridines and their application as corrosion inhibitors at C60 steel, *J. Chem. Sci.*, 2009, **121**, 693–701.

32 Allen J. Bard and Larry R. Faulkner, *Electrochemical Methods: Fundamentals and Applications, New York: Wiley, 2001, 2nd ed.*, 2002, vol. 38.

33 T. Itakura, R. Sasai and H. Itoh, Arsenic recovery from water containing arsenite and arsenate ions by hydrothermal mineralization, *J. Hazard. Mater.*, 2007, **146**, 328–333.

34 J. Á. Menéndez Díaz, Electrical charge distribution on carbon surfaces as a function of the pH and point of zero charge. An approximate solution.

35 S. Wei, S. Li, R. Wei, S. Liu and W. Du, Different morphologies of WO3 and their exposed facets-dependent acetone sensing properties, *Sensors Actuators B Chem.*, 2021, **329**, 129188.

36 W. P. Zhou, L. A. Kibler and D. M. Kolb, XPS study of irreversibly adsorbed arsenic on a Pt(111) electrode, *Electrochim. Acta*, 2004, **49**, 5007–5012.

37 A. Dutta, M. M. Hasan, M. R. Miah, Y. Nagao and M. A. Hasnat, Efficient sensing of hydrogen peroxide via electrocatalytic oxidation reactions using polycrystalline Au

electrode modified with controlled thiol group immobilization, *Electrochim. Acta*, , DOI:10.1016/J.ELECTACTA.2021.139217.

38 Q. Zhang and H. Wang, Facet-dependent catalytic activities of Au nanoparticles enclosed by high-index facets, *ACS Catal.*, 2014, **4**, 4027–4033.

39 Y. Kang, S. M. João, R. Lin, K. Liu, L. Zhu, J. Fu, W.-C. Cheong, S. Lee, K. Frank and B. Nickel, Effect of crystal facets in plasmonic catalysis, *Nat. Commun.*, 2024, **15**, 3923.

40 Z. Liu, B. Xu, X. Lu, P. Li, J.-J. Zhu and W. Zhu, Understanding Au facet effects in photocatalytic nonoxidative coupling of methane, *Mater. Chem. Front.*

41 F. Garcia-Martinez, C. García-Fernández, J. P. Simonovis, A. Hunt, A. Walter, I. Waluyo, F. Bertram, L. R. Merte, M. Shipilin and S. Pfaff, Catalytic Oxidation of CO on a Curved Pt (111) Surface: Simultaneous Ignition at All Facets through a Transient CO-O Complex, *Angew. Chemie*, 2020, **132**, 20212–20218.

42 U. T. Ndongmouo, F. Hontinfinde and R. Ferrando, Numerical study of the stability of (111) and (331) microfacets on Au, Pt, and Ir (110) surfaces, *Phys. Rev. B*, 2005, **72**, 115412.

43 H. Katz-Boon, M. Walsh, C. Dwyer, P. Mulvaney, A. M. Funston and J. Etheridge, Stability of crystal facets in gold nanorods, *Nano Lett.*, 2015, **15**, 1635–1641.

44 M. Zhu, B. Lei, F. Ren, P. Chen, Y. Shen, B. Guan, Y. Du, T. Li and M. Liu, Branched Au Nanostructures Enriched with a Uniform Facet: Facile Synthesis and Catalytic Performances, *Sci. Rep.*, 2014, **4**, 5259.

45 D. Briggs, *Handbook of X-ray Photoelectron Spectroscopy*, John Wiley & Sons, Ltd, 1981, vol. 3.

46 N. H. Turner and A. M. Single, Determination of peak positions and areas from wide-scan XPS spectra, *Surf. Interface Anal.*, 1990, **15**, 215–222.

47 M. P. Casaletto, A. Longo, A. Martorana, A. Prestianni and A. M. Venezia, XPS study of supported gold catalysts: the role of Au0 and Au+ δ species as active sites, *Surf. Interface Anal. An Int. J. devoted to Dev. Appl. Tech. Anal. surfaces, interfaces thin Film.*, 2006, **38**,

215–218.

48 A. G. Shard, Practical guides for x-ray photoelectron spectroscopy: Quantitative XPS, *J. Vac. Sci. Technol. A*.

49 D. Reyter, D. Bélanger and L. Roué, Study of the electroreduction of nitrate on copper in alkaline solution, *Electrochim. Acta*, 2008, **53**, 5977–5984.

50 M. R. Miah, J. Masud and T. Ohsaka, Kinetics of oxygen reduction reaction at electrochemically fabricated tin-palladium bimetallic electrocatalyst in acidic media, *Electrochim. Acta*, 2010, **56**, 285–290.

51 E. Chrzescijanska, E. Wudarska, E. Kusmierek and J. Rynkowski, Study of acetylsalicylic acid electroreduction behavior at platinum electrode, *J. Electroanal. Chem.*, 2014, **713**, 17–21.

52 C. Brett and A. M. O. Brett, *Electrochemistry: principles, methods, and applications*, Oxford University Press, 1993.

53 Z. Mumtarin, M. M. Rahman, H. M. Marwani and M. A. Hasnat, Electro-kinetics of conversion of NO3− into NO2− and sensing of nitrate ions via reduction reactions at copper immobilized platinum surface in the neutral medium, *Electrochim. Acta*, 2020, **346**, 135994.

54 M. A. Bhat, P. P. Ingole, V. R. Chaudhari and S. K. Haram, Outer sphere electroreduction of CCl4 in 1-butyl-3- methylimmidazolium tetrafluoroborate: An example of solvent specific effect of ionic liquid, *J. Phys. Chem. B*, 2009, **113**, 2848–2853.

55 M. Tarikul Islam, M. Imran Hossain, K. Aoki, Y. Nagao, M. Mahmudul Hasan, M. Rahaman, A. Aldalbahi and M. A. Hasnat, Electrochemical Reduction of CO2 by the SnS| PTFE| Pt Surface in an Aqueous Imidazole Medium: Catalysis and Kinetics, *ACS Appl. Energy Mater.*, , DOI:10.1021/acsaem.3c03142.

56 M. A. Hasnat, M. M. Hasan, N. Tanjila, M. M. Alam and M. M. Rahman, pH dependent kinetic insights of electrocatalytic arsenite oxidation reactions at Pt surface, *Electrochim. Acta*, 2017, **225**, 105–113.

57 X. Dai and R. G. Compton, Detection of As(iii) via oxidation to As(v) using platinum nanoparticle modified glassy carbon electrodes: arsenic detection without interference from copper, *Analyst*, 2006, **131**, 516–521.

58 S. Hrapovic, Y. Liu and J. H. T. Luong, Reusable Platinum Nanoparticle Modified Boron Doped Diamond Microelectrodes for Oxidative Determination of Arsenite, *Anal. Chem.*, 2007, **79**, 500–507.

Data Availability Statement

All the data have been reported in the manuscript.